Analysis of noise exciting magnetic force waves by means of numerical simulation and a space vector definition

M. van der Giet, R. Rothe, M. Herranz Gracia and K. Hameyer
Institute of Electrical Machines, RWTH Aachen University, Germany
Email: Michael.vanderGiet@IEM.RWTH-Aachen.de

***Abstract*—This paper presents a combined analytical and numerical approach to identify and accurately compute the magnetic force excitation in electrical machines. The method is based on convolution of airgap fields. Space vectors are used to visualize the results. The presented approach is applied to three different types of rotating field machines: a BLDC, and IPMSM and an induction motor drive.**

I. Introduction

The reduction of audible noise in electrical machines is attracting more and more attention. For being able to design low noise electrical machines, a good understanding of the causes of noise excitation is essential.

Classical analytical approaches for noise analysis in electrical machines rely on the identification of space and time harmonics of the airgap field that generate radial magnetic force waves [1], [2]. With analytical models, the causality relation between a given force wave and the field harmonics from which it originates can be traced back without ambiguity. Their drawback, however, is the limited accuracy of the airgap field and magnetic force wave amplitudes, as well as the fact that the influence of specific properties of the magnetic circuit, such as details of the stator outer contour cannot be considered.

Numerical simulations, with e.g. the Finite Element method, are able to capture finer details and allow an accurate determination of airgap field and magnetic force amplitudes [2], [3] and [4]. However, because they take e.g. saturation into account, they are unable to readily establish causality relations between field waves and force waves. The method proposed in this paper overcomes this difficulty by establishing a link between the analytical and the numerical approach.

The approach is applied to three problems: The quantitative analysis of the influence of stator shape modifications on the acoustic behavior of an induction machine (IM). As a second example, the influence of the current waveform on the acoustic behavior of a BLDC motor drive is analysed. Finally, the method is used to investigate the influence of field-weakening on the vibration of an IPMSM.

II. Generation of Magnetic force density Components

The airgap field in electrical machines represents the magnetic energy that acts as forces densities on the permeable material of the stator and rotor teeth. Featuring different frequency components, these forces are responsible for mechanical vibrations that radiate air-borne sound. Provided the airgap field is known, the radial magnetic force density component can be approximated by the simplified Maxwell stress tensor (SMST) equation

$$p^r(x,t) = \frac{b^n(x,t)}{2\mu_0}. \tag{1}$$

The airgap field is periodic in time and space and it can be expressed as Fourier series of a one-dimensional wave by

$$b(x,t) = \sum_{i=0}^{\infty} \hat{B}_i \cos(r_i x - \omega_i t - \Psi_i). \tag{2}$$

Applying (1) gives

$$\begin{aligned} p^r(x,t) &= \frac{1}{2\mu_0}\left[\sum_{j=1}^{\infty} \hat{B}_j \cdot \cos(\nu_j x - \omega_j t - \Psi_j)\right]^2 \\ &= \frac{1}{2\mu_0}\sum_{k=1}^{\infty}\sum_{l=1}^{\infty} \hat{B}_k\hat{B}_l \cdot \cos(\nu_k x - \omega_k t - \Psi_k) \\ &\quad \cdot \cos(\nu_l x - \omega_l t - \Psi_l) \\ &= \frac{1}{2\mu_0}\sum_{k=1}^{\infty}\sum_{l=1}^{\infty} \frac{\hat{B}_k\hat{B}_l}{2} \\ &\quad \cdot \cos((\nu_l \pm \nu_k)x - (\omega_l \pm \omega_k)t - \Psi_l \pm \Psi_k). \\ &= \sum_{k=1}^{\infty}\sum_{l=1}^{\infty} \hat{P_{kl}} \cdot \cos(r_{kl}x - \omega_{kl}t - \Psi_{kl}) \end{aligned} \tag{3}$$

Airgap field components combine magnetic force density components two by two, whereas the amplitude and the ordinal numbers are

$$\hat{P_{kl}} = \frac{\hat{B}_k\hat{B}_l}{2}, \quad r_{kl} = \nu_l \pm \nu_k, \quad \omega_{kl} = \omega_l \pm \omega_k. \tag{4}$$

A common method to analyze magnetic force density components is Jordan's combination table [1].

In such a full analytical approach, the air gap field $b(x,t)$ is calculated from the permeance function of the machine and the magnetomotive force (MMF). As shown in Table I, a variety

TABLE I
Ordinal numbers of typical airgap field components.

Factor	No. of pole pair	Frequency
Stator slotting	$gN_1 + p, g \in \mathbb{N}$	f_p
Rotor slotting (IM)	$gN_2 + p, g \in \mathbb{N}$	$f_p(1 + \frac{gN_2}{p}(1-s))$
Stator wind. distr.	$p(6g+1), g \in \mathbb{Z}$	f_p
Current harmonic μ	$p(6g+\mu), g \in \mathbb{Z}$	μf_p
Saturation	3p	$3f_p$

978-1-4244-1736-0/08/$25.00 ©2008 IEEE

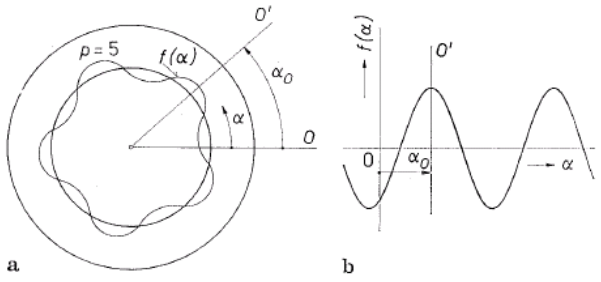

Fig. 1. General illustrations of one-dimensional harmonic waves,(a) wave with p=5, (b) value along angle, from [5]

of typical air gap field components can be derived in this way. The ordinal numbers of components arising from stator or rotor slotting, winding distribution or saturation are well known and described by the number of stator and rotor teeth N_1 and N_2, the number of pole pairs p, the frequency of the fundamental component f_p. Simplifying assumptions and hardly predictable effects like saturation diminish the accuracy of quantitative statements concerning the amplitude of higher harmonics. In addition, depending on the kind of machine. It happens in pratice that force density harmonics are measured or simulated with FE analysis that cannot be identified using the analytical model. Their true origin therefore remains unknown.

III. Analysis of Magnetic force density Components using Numerical Simulation Data

In contrast to the analytical derivation of the airgap field, a two-dimensional electromagnetic FEM simulation provides an accurate representation of the magnetic flux density distribution in the machine. The airgap field can be sampled in time and space and the Fourier series components subsequently approximated by means of the discrete Fourier transformation (DFT) components. Since many air gap field component combinations have the same ordinal numbers, a magnetic force density component is usually the geometrical sum of a number of pairs of airgap field components. This can be illustrated with space vector diagrams introduced in this section.

A. Concept of Space Vectors

Space vectors are frequently used as a tool to describe and calculate the flux model of controlled machines under various operation modes. However, space vectors offer also a more general description for arbitrary one-dimensional harmonic waves in electrical machines. A graphic definition of space vectors defined as complex numbers was first proposed for electrical machines by Kovcs and Štěpina. It allows a handling of harmonic waves in a convenient way [5]. A single harmonic wave can be expressed by

$$\begin{aligned} f(\alpha) &= F_p \cdot \cos[p(\alpha-\alpha_0)+\omega(t-t_0)] \\ &= F_p \cdot Re\{e^{j(p\alpha_0+\omega t_0)}e^{-j(p\alpha+\omega t)}\}. \end{aligned} \tag{5}$$

The space vector is defined as the complex number

$$\underline{F} = F_p \cdot e^{j(p\alpha_0+\omega t_0)}. \tag{6}$$

In this way, airgap field and magnetic force waves can be described by rotating vectors in the complex plane. The magnitude of the vector corresponds to the wave amplitude, whereas the angle corresponds to the phase shift as depicted in Fig 1.

B. Convolution Approach

In the sampling procedure, a full period of the FEM solution data is stored to a sampling matrix $\mathbf{B}(x,t)$. In order to consider the magnetic force density components, the magnetic force density matrix $\mathbf{p}(x,t)$ is created by applying (1) to each matrix entry. Subsequently, a two-dimensional DFT of $\mathbf{p}(x,t)$ provides the approximated Fourier series components. Path (I) in Fig. 2 illustrates this approach. Matrix $\mathbf{p}_{DFT2}(r,f)$ contains space vectors of harmonic magnetic force waves.

Path (II) in Fig. 2 indicates an alternative way of calculating magnetic force density components $\mathbf{p}_{DFT2}(r,f)$. Primarily, the two-dimensional DFT is applied directly to the airgap field matrix $\mathbf{B}$. Then, a periodic matrix convolution allows for a calculation of $\mathbf{p}_{DFT2}(r,f)$. The two-dimensional periodic DFT is defined by

$$\begin{aligned} z_{k,l} &= y_{m,n} * y_{m,n} \\ &= \frac{1}{MN}\sum_{m=0}^{M-1}\sum_{n=0}^{N-1} y_{m,n}\cdot y_{k-m,l-n}\ , \end{aligned} \tag{7}$$

Applied to the airgap field DFT matrix, a periodic matrix convolution combines all matrix entries with each other. This can be abbreviated by

$$\mathbf{p}_{DFT2}(r,f) = \frac{1}{2\mu_0}\cdot\mathbf{B}_{DFT2}(\nu,f) * \mathbf{B}_{DFT2}(\nu,f). \tag{8}$$

This approach seems to be complex and costly.

But in contrast to path (I), an advantage arises from the fact that each airgap field convolution pair is known and can be stored. A complete unabridged convolution (8) performed by a computer routine would however be very time consuming. But in fact, a complete convolution is not necessary since only a very small number of combination pairs do contribute significantly to the magnetic force density component that really cause audible noise. Therefore, only the matrix entries of $\mathbf{B}_{DFT2}$ are singled out whose amplitude exceed a chosen threshold.

C. Space Vector Diagram

Following the convolution approach, an arbitrary magnetic force component can be split into the geometric addition of

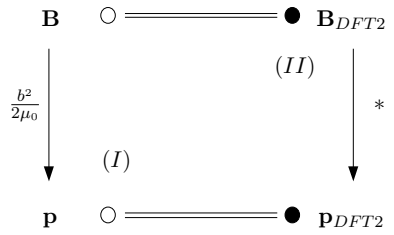

Fig. 2. Derivation of magnetic force matrices.

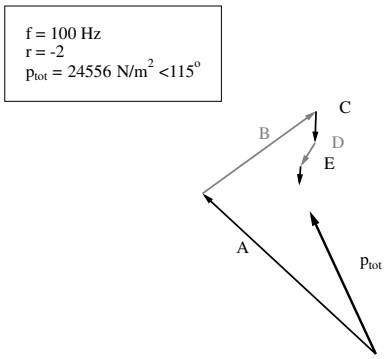

Fig. 3. Space vector diagram for $f = 100Hz$ and $r = -2$.

TABLE II
CONTRIBUTING AIRGAP FIELD COMPONENTS.

Vector	f(Hz)	ν	f (Hz)	ν
A	100	-2	200	-4
B	200	-4	300	-6
C	50	-1	150	-3
D	150	-3	250	-5
E	50	-1	50	-1

partial space vectors as shown in Fig. 3. The depicted magnetic force density component has mode number $r = -2$ and and a frequency of $f = 100$ Hz. Each of the partial vectors A, B, C etc. is associated with an airgap field combination pair. The thick phasor is the total magnetic force density component calculated using path (I). Obviously, the chain of partial vectors adds up to the total component except for a remaining gap that depends on the chosen convolution threshold and on the number of stored partial vectors. Table II lists the ordinal numbers of the combining airgap field components for each partial space vector.

The ordinal numbers of Table II must be added or subtracted to obtain 100Hz and $r = -2$ according to (4).

D. Identification of Airgap Field Components

To establish a link between disturbing radiated acoustic frequencies and responsible factors, it is necessary to trace back the origin of the airgap field components of Table II. Since known components with high amplitudes (Table I) are frequently responsible for noise, they can easily be identified by their ordinal numbers. The causes of others remain unknown. But additional FEM simulations could allow for an identification. In FEM analysis it is possible to switch factors, e.g. holes or notches, by varying the material parameters. A reference FEM experiment can be compared to a second one experiment where factors like a notch or a magnet failure in the rotor have been modified. This approach could help identifying the origin of the partial space vectors that were not found in Jordan's combintation table.

IV. NUMERICAL RESULTS

A. Analysis of synchronous machines

1) Brushless DC motor drive: The BLDC motor under analysis is a 500 W, six pole machine with 9 stator slots designed as a variable speed drive.

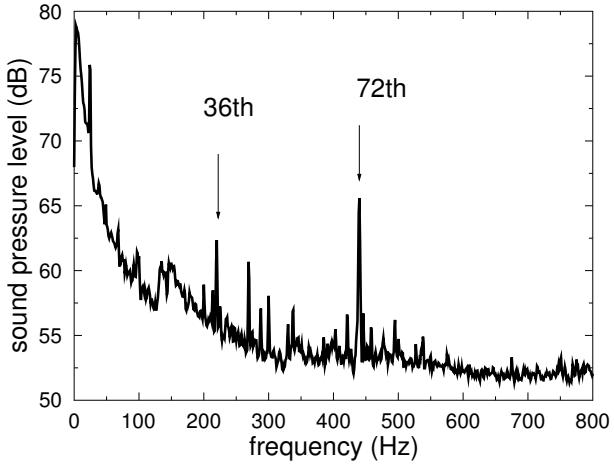

Fig. 4. Measured sound pressure level.

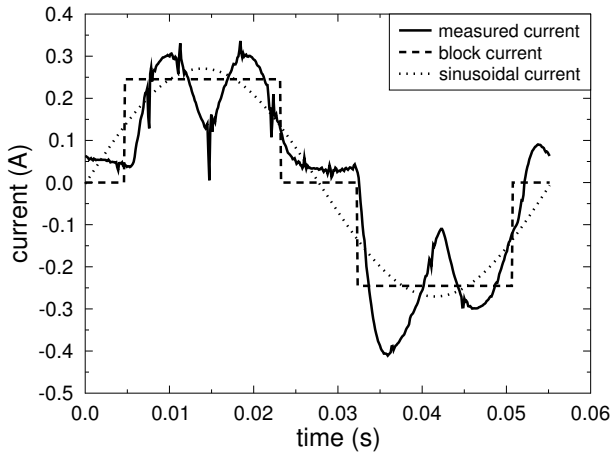

Fig. 5. Comparison of current waveforms.

Laboratory tests evidented disturbing audible single tones at some speeds, which are most probably due to resonances of mode zero of the supporting mechanical structure. Fig 4 shows airborne sound for n=367 1/min. The 36^{th} and 72^{th} order of mechanical speed can be clearly identified as disturbing single tones. By means of analytical approach [6], it is possible to show that current time harmonics are involved in the generation of these frequencies. It however, does not provide any quantitative statement about the influence of the current harmonics on the magnetic force.

For cost reasons, the BLDC is not equipped with a feedback current control loop, which would require accurate current sensing. Therefore, the BLDC is operated in open loop voltage control. This leads to additional current harmonics when compared to a pure rectangular current waveform. So the question is, whether the additional current harmonics are the reason for the disturbing noise. There are three options which are considered for the current excitation: Pure sine wave current, e.g. by means of a PWM converter, a pure rectangular current waveform and the measured current resulting from the open loop voltage supply. For n=367 1/min, the current waveforms and spectra are shown in Fig. 5 and 6 , respectively.

Applying 2D FEM analysis to this problem problem yields

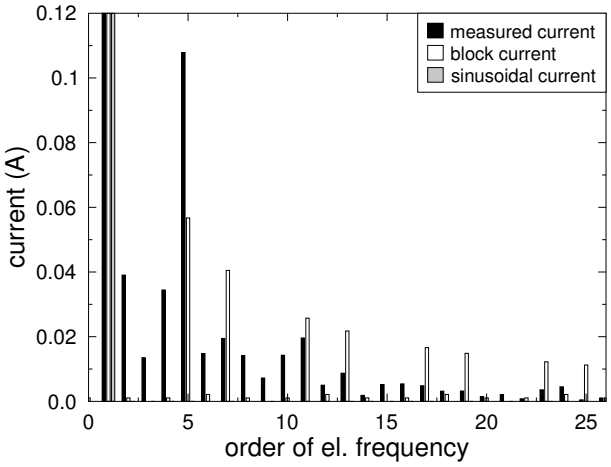

Fig. 6. Spectral comparison of current (fundamental of approx. 0.3A not shown).

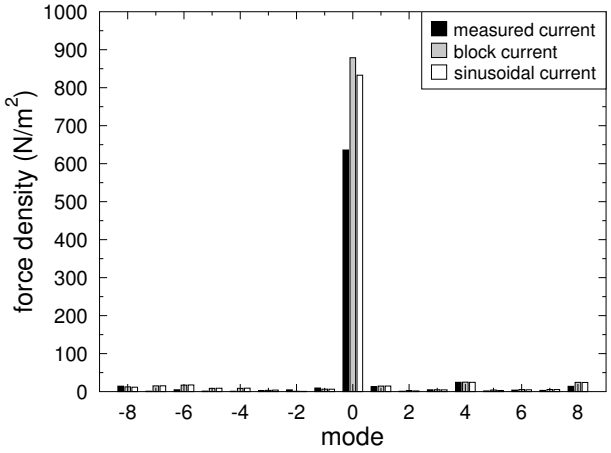

Fig. 7. Force excitation at 36^{th}order of mechanical speed.

the force excitation modal distribution, as shown in Fig. 7 and 8. It can be seen that for the 36^{th} order the measured current actually represents the best option in terms of force excitation. For the 72^{th} order, sinusoidal supply current is clearly the best choice. It remains the question, why does the open loop voltage supply lead to less noise for the 36^{th} order and why does the rectangular current supply give so large force excitations.

Applying the proposed convolution approach the space vector diagrams in Fig. 9 and 10 are obtained for measured currents and sinusoidal current supply, respectively. For the 36^{th} order, It can be seen that the individual force contributions only very slightly between the two excitation types, however the phase angle varies significantly and result in a lower total force for the measured current excitation. The sensitivity of force excitation to current harmonics together with the possibility to precisely study their influence gives allows for an optimization of current with respect to noise, which however is not subject here. For the 72^{th} order, the resulting space vector data are given in Fig. 11 and 12 for measured currents and block currents, respectively. It can be seen that in the most significant contributions to the force excitation with the measured currents are the 416 Hz and 453 Hz components

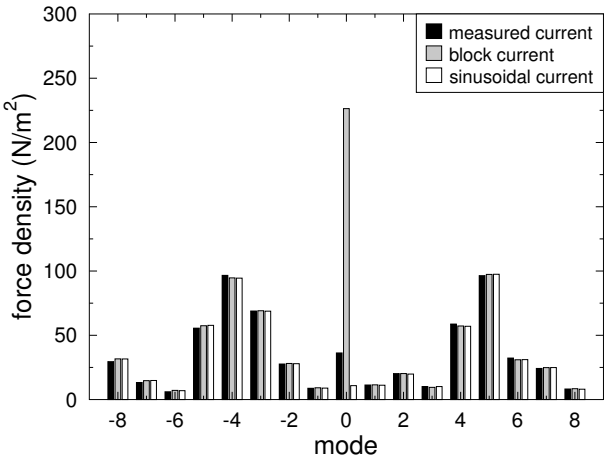

Fig. 8. Force excitation at 72^{th}order of mechanical speed.

f = 217 Hz
r = 0
p_{tot} = 636 N/m^2 < -172°

Vector	f1,nu1	f2,nu2
A	18Hz,33	199Hz,-33
B	18Hz,-3	199Hz,3
C	54Hz,27	163Hz,-27
D	18Hz,-3	235Hz,-3
E	54Hz,-9	163Hz,9
F	18Hz,-39	235Hz -39

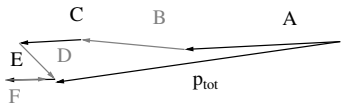

Fig. 9. Space vector diagram with measured currents at 36^{th}order of mechanical speed.

f = 217 Hz
r = 0
p_{tot} = 836 N/m^2 < -175°

Vector	f1,nu1	f2,nu2
A	18Hz,-3	199Hz,3
B	18Hz,33	199Hz,-33
C	54Hz,27	163Hz,-27
D	54Hz,-9	163Hz,9
E	18Hz,-39	235Hz,-39
F	18Hz,-3	235Hz,-3

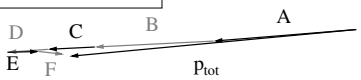

Fig. 10. Space vector diagram with sinusoidal currents at 36^{th}order of mechanical speed.

f = 434 Hz
r = 0
p_{tot} = 36 N/m^2 < -76^o

Vector	f1,nu1	f2,nu2
A	18Hz,-3	416Hz,3
B	18Hz,-3	453Hz,-3
C	18Hz,-75	453Hz,-75
D	18Hz,69	416Hz,-69
E	54Hz,-9	380Hz,9
F	127Hz,51	308Hz,-51

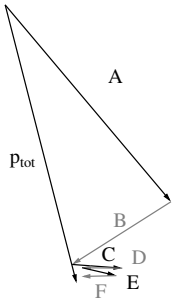

Fig. 11. Space vector diagram with measured currents 72thorder of mechanical speed.

f = 434 Hz
r = 0
p_{tot} = 226 N/m^2 < 78^o

Vector	f1,nu1	f2,nu2
A	18Hz,-3	416Hz,3
B	18Hz,-3	453Hz,-3
C	54Hz,-9	380Hz,9
D	18Hz,-75	453Hz,-75
E	18Hz,69	416Hz,-69
F	127Hz,51	308Hz,-51

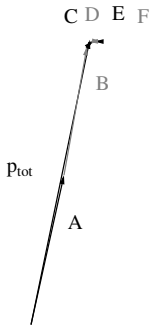

Fig. 12. Space vector diagram with block currents 72thorder of mechanical speed.

with $\nu = 3 = p$.

From Table I, it can be seen that these can only stem from stator current harmonics of $\mu = 23$ and 25, respectively. The space vector diagram shows that for the case with measured currents, vector A and and B are in perpendicular, where they are much larger and in phase in case of rectangular currents. This can be confirmed by the current spectrum Fig. 6, as the measure current as much lower harmonic components for $\mu =$ 23 and 25 than the block current.

The analysis showed that the single tones are not due to, but in fact are even lower, for the open loop voltage supply compared to a close loop current regulation.

2) IPMSM: The developed convolution and space vector approach is applied to the vibration problem of an interior permanent magnet synchronous machine (IPMSM) with eight magnets and 18 stator slots. As it is used over a wide speed range with limited supply voltage, field-weakening operation is required. On the test bench, it is found that the supply voltage and therefore the degree of field-weakening has a significant influence on the acoustic behavior of the machine.

In base speed operation, current leads the d-axis by an angle of 90^o. For field-weakening, a demagnetization is required and can be achieved by the current leading the d-axis by an angle more than 90^o. The angle between current and the q-axis is defined as

$$\gamma = \beta - \frac{\pi}{2}\,, \tag{9}$$

where β is the angle between current and the d-axis [7]. In this case, for base speed operation, $\gamma = 25^o$, and for field-weakening $\gamma > 25^0$, since reluctance, which is due to siliency, is utilized.

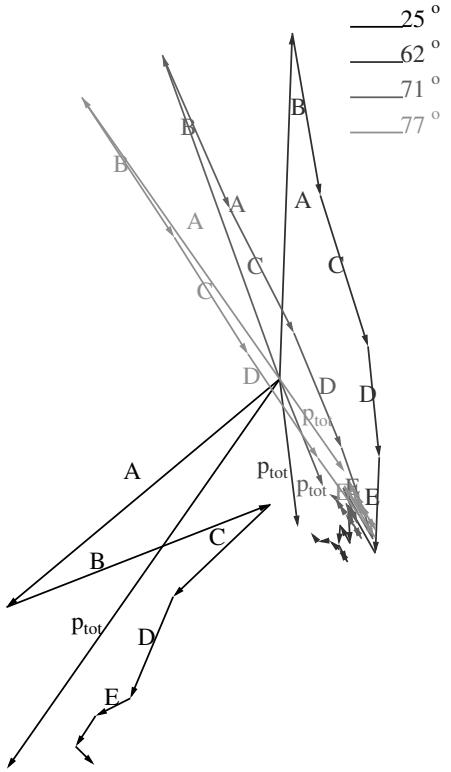

Fig. 13. Space vector diagram of force excitation for different values of γ for $r = 2$ and 16thorder.

The field distribution in the machine is computed using FE simulation for different speeds above base speed. The Fourier decomposition of the electromagnetic forces shows that the important orders of mechanical frequency strongly depend on γ. For the 8^{th} and 16^{th} order, the force excitation with critical modes numbers decrease with γ. The force excitations of 24^{th} and 48^{th} order increase with γ, however these excitations are in most cases not cortical, since they are excited with mode number 6, which is comparatively large. For the 32^{th} and 56^{th} order, the force excitation is strongly increased for mode 8, slightly increased for mode 2 and decreased for mode 4 with γ.

For the analysis of this behavior, the convolution approach is applied and results are shown in Fig. 13 and in Table III exemplary for $r = 2$ and the 16^{th}order of mechanical frequency for different values of γ.

The magnitude of force waves, to which the fundamental field component contributes, are reduced with increasing γ. This can be seen, e.g. from lines 1, 8, 13 and 18 in Table III, where the magnitude of the force wave decreases from $8109\frac{\text{N}}{\text{m}^2}$ to $3145\frac{\text{N}}{\text{m}^2}$. Excitations, in which the fundamental field component is not involved, vary slightly, possibly due to less saturation for increasing field-weakening, see e.g. lines 2,6,11 and 16. However, it can be said that the reduction of the fundamental field dominates the force excitation and therefore the total force excitation decreases with increasing to γ. It shows that the decomposition of force excitations by means

TABLE III
FORCE DENSITY EXCITATION SPACE VECTORS FOR $r = 2$ AND 16^{TH} ORDER.

γ	No.	Vec.	$\hat{p_k}\left(\frac{\text{N}}{\text{m}^2}\right)$	φ_k	ν_1	ord.	ν_2	ord.
25^o	1	A	8109	-140^o	4	4	-6	12
	2	B	6454	21^o	-14	4	12	12
	3	C	3058	-136^o	4	4	2	20
	4	D	2513	-113^o	22	4	20	20
	5	E	885	-153^o	-32	4	30	12
62^o	6	A	7891	88^o	-14	4	12	12
	7	B	3756	-80^o	22	4	20	20
	8	C	3606	-72^o	4	4	-6	12
	9	D	2540	-84^o	12	12	10	28
	10	E	2189	-92^o	4	4	2	20
71^o	11	A	7850	110^o	-14	4	12	12
	12	B	3819	-66^o	22	4	20	20
	13	C	3189	-63^o	4	4	-6	12
	14	D	2831	-67^o	12	12	10	28
	15	E	2201	-71^o	4	4	2	20
77^o	16	A	7845	125^o	-14	4	12	12
	17	B	3824	-57^o	22	4	20	20
	18	C	3145	-58^o	4	4	-6	12
	19	D	2860	-56^o	12	12	10	28
	20	E	2215	-54^o	4	4	2	20

of the proposed approach also yields more insight into the generation process of force waves for the field weakening of IPMSM.

B. Sensibility analysis of induction machine

The sensibility of the stator deformation of an induction machine (IM) with a nominal power of 500W with respect to small geometry variations is studied. The machine has two pole pairs and the number of rotor slots is $N_2 = 26$. The sensibility analysis is performed numerically through coupled electromagnetic and mechanical 2D simulations. The body-sound index $L(f)$, an integral value related to the deformation of a body, is used as evaluation variable. It is defined as the sum of the square of the normal component of the velocity of deformation $|\vec{v} \cdot \vec{n}|$ for all the finite elements p in the surface S of the body:

$$L(f) = 10 \cdot \log\left(\frac{\sum_p \int_{S_p} |\vec{v_p} \cdot \vec{n^p}|^2 \mathrm{d}S}{S_0 \cdot h_{U_0}^2}\right) \qquad (10)$$

$S_0 = 1\mathrm{m}^2$ and $h_{U_0}^2 = 250 \cdot 10^{-15}\mathrm{m}^2$ are reference values.

The phasor diagrams of the stator force density are studied in the last step to ensure the causal link between the geometry parameters and the obtained numerical results.

Three geometry parameters, which are changed from its nominal value to zero, are considered:

- Depth of the mounting notches
- Depth of the welding notches
- Depth of the stamping notches

The results are compared for the frequencies corresponding to the first and second rotor slot harmonic. They are shown in Table IV. It can be observed that the second rotor slot harmonic is strongly worsened due to the mounting and the stamping notches.

The causality link between the deformation with the frequency of the 2^{nd} rotor slot harmonic and the mounting and stamping notches can be found using the phasor diagrams of the force density excitation at this frequency. Particularly the one with mode number $r = 2$ show some significant components, which can be analytically identified as caused by the stamping and the mounting notches.

TABLE IV
RESULTS OF THE SENSIBILITY ANALYSIS OF THE IM.

Geometry Variation	Variation of the body-sound index	
	1^{st} rotor slot harmonic	2^{nd} rotor slot harmonic
Mounting notches	-0.2 dB	+6.5 dB
Welding notches	+0.2 dB	2 dB
Stamping notches	+0.2 dB	+7 dB

V. SUMMARY AND CONCLUSIONS

This paper proposes an approach to accurately determine the magnitude and to identify the cause for force waves in the airgap of electrical machines. It is based on the convolution of airgap field components determined from 2D FEA. The results are represented using a space vector definition.

Numerical results are shown for three different machines: For a BLDC, the influence of current harmonic on the force waves is studied. Second, the correlation between force excitation and field weakening is studied for a IPMSM, and finally the influence of stator modification of an IM are investigated and causality relation are. established.

In general, it can be said that the proposed convolution approach helps to understand the generation of force excitations in rotating field machines. The approach allows for a splitting of forces into their contributing field components. One step, which is left for future work, is the establishment of a decomposition of the field itself according to the field producing entities in the machine. This could e.g. being solved by using frozen permeabilites.

REFERENCES

[1] H. Jordan, *Geräuscharme Elektromotoren*, H. Franz, Ed. W. Girardet, November 1950.

[2] J. Gieras, C. Wang, and J. C. Lai, *Noise of Polyphase Electric Motors*. CRC Press Taylor&Francis Group, 2006.

[3] M. Furlan, A. Cernigoj, and M. Boltezar, "A coupled electromagnetic-mechanical-acoustic model of a dc electric motor," *COMPEL: The International Journal for Computation and Mathematics in Electrical and Electronic Engineering*, vol. 22, no. 4, pp. 1155–1165, 2003.

[4] C. Schlensok, B. Schmülling, M. van der Giet, and K. Hameyer, "Electromagnetically excited audible noise evaluation and optimization of electrical machines by numerical simulation," *COMPEL: The International Journal for Computation and Mathematics in Electrical and Electronic Engineering*, vol. 26, pp. 727 – 742, 2007.

[5] J. Štěpina, "Komplexe Größen in der Elektrotechnik," *Electrical Engineering (Archiv für Elektrotechnik)*, vol. 72, no. 6, pp. 407–414, November 1989.

[6] Z. Zhu and D. Howe, "Electromagnetic noise radiated by brushless permanent magnet dc drives," in *Electrical Machines and Drives, 1993. Sixth International Conference on (Conf. Publ. No. 376)*, 1993, pp. 606–611.

[7] T. J. E. Miller, *Brushless Permanent-Magnet and Reluctance Motor Drives (Monographs in Electrical and Electronic Engineering)*. Oxford University Press, USA, 6 1989. [Online]. Available: http://amazon.com/o/ASIN/0198593694/